

## Finding a needle in a chemical haystack: tip-enhanced Raman scattering for studying carbon nanotubes mixtures

This article has been downloaded from IOPscience. Please scroll down to see the full text article.

2010 Nanotechnology 21 445704

(<http://iopscience.iop.org/0957-4484/21/44/445704>)

View [the table of contents for this issue](#), or go to the [journal homepage](#) for more

Download details:

IP Address: 81.149.206.37

The article was downloaded on 05/11/2010 at 11:33

Please note that [terms and conditions apply](#).

# Finding a needle in a chemical haystack: tip-enhanced Raman scattering for studying carbon nanotubes mixtures

K L Andrew Chan and Sergei G Kazarian

Department of Chemical Engineering, Imperial College London, SW7 2AZ, UK

E-mail: [s.kazarian@imperial.ac.uk](mailto:s.kazarian@imperial.ac.uk)

Received 5 August 2010, in final form 31 August 2010

Published 8 October 2010

Online at [stacks.iop.org/Nano/21/445704](http://stacks.iop.org/Nano/21/445704)

## Abstract

Tip-enhanced Raman scattering (TERS) has emerged as a powerful analytical tool for measuring chemical images with nanometre spatial resolution. In this paper, the application of TERS to study differentiation of single-walled carbon nanotubes (SWCNTs) with 14 nm spatial resolution is demonstrated by the measurement of a mixture of two different types of SWCNTs as the model sample. The results demonstrate that TERS is a viable tool for the detection and localization of different SWCNTs and amorphous carbon in mixed SWCNTs based on the spectral differences in the radial breathing mode and the D bands.

(Some figures in this article are in colour only in the electronic version)

## 1. Introduction

Raman microscopy is a powerful and valuable material characterization method. Chemical images with Raman spectroscopy can be obtained by mapping point by point across a sample. The spatial resolution is limited by diffraction with a lateral resolution of  $\sim 0.5 \mu\text{m}$  when measured in far-field confocal mode. To break the diffraction limit, a different approach has recently been developed by taking the advantage of surface-enhanced Raman spectroscopy (SERS), which was discovered more than 30 years ago [1], and atomic force microscopy (AFM). Tip-enhanced Raman scattering (TERS) has emerged as a promising technique that offers both rich chemical information and nanometre spatial resolution [2–6]. The idea of this approach is to probe samples using the surface-enhanced Raman effects at the apex of a sharp AFM tip. Nanometre spatial resolution can be achieved by the extreme localized enhancement effect [7, 8]. Spatial resolution of  $\sim 4 \text{ nm}$  has been reported based on spectral shift of the G band of SWCNT when localized contact pressure was applied to the nanotube [9]. This opens up many opportunities in material analysis with vibrational spectroscopy for samples with nanoscale size domains. The synthesis of carbon nanotubes is a complicated process and impurities, such as other carbonaceous materials, are sometimes formed in the process [10, 11]. It has been shown that it is possible to

provide the complete atomic structural assignment of SWCNT based on the radial breathing mode (RBM) vibrational frequency [12]. Another work has demonstrated the chirality changes in SWCNT with 40 nm spatial resolution based on both the SWCNT G bands and RBM vibrations [13]. In this work, we demonstrate the possibility of detecting and locating different impurities in SWCNT bundles as well as differentiating a range of SWCNTs using TERS. Because of the small distances between the SWCNTs, their differentiation could not be performed using conventional Raman microscopy or imaging. Carbon nanotubes of different chiralities and diameters,  $d_t$ , have been deliberately mixed and used as model samples for this purpose. We also report on our approaches in a TERS study using a commercial instrument [6] and the difference in performance on newly coated and recoated AFM tips.

## 2. Experimental details

TERS images were obtained with an inverted microscope with 100 $\times$  oil immersion objective (NA of 1.3, Olympus), a Raman spectrometer (nVia Raman Microscope, Renishaw, UK) with 633 nm HeNe laser, a circular polarizer (Renishaw, UK) and a 1024 pixels  $\times$  400 pixels CCD (Andor detector) connected to an AFM system (NTEGRA Spectra, NT-MDT). Contact mode Si AFM tips (CSG10, NT-MDT) were sputtered with a thin layer

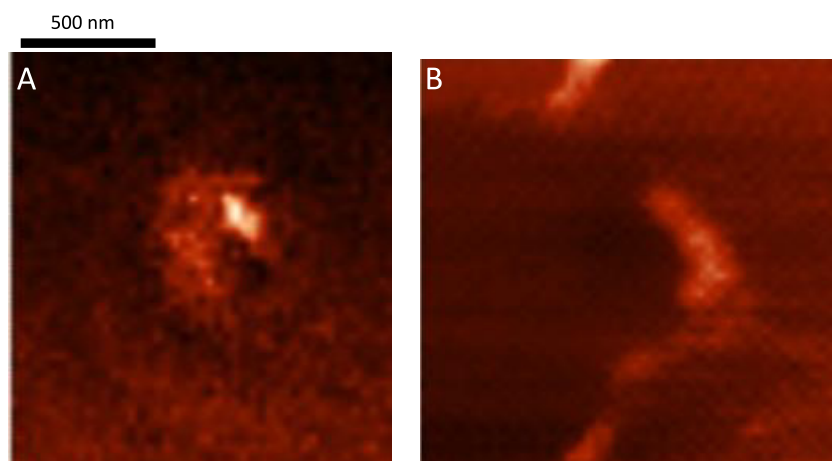


**Figure 1.** (A) Image of a hot spot based on the G band of SWCNT. (B) AFM topography measured simultaneously during scanning for the hot spot.

of gold coating (K550X, Emitech, Quorum Technologies, UK) under the condition of  $10^{-1}$  mbar of argon, coating current of 35 mA, 45 mm distance from the sputtering source and 2 min of coating time. The soft piezo-approach technique was adapted to avoid damage to the gold on the tip and the lowest contact pressure settings were used to minimize the impact between the tip and sample. A laser beam with a power of  $\sim 0.01$  mW was focused on the sample and the apex of the gold-coated AFM tip. A 0.3 s integration time was used to collect the Raman signal at each point of the map and data were collected at a rate of  $\sim 3$  spectra  $s^{-1}$ . Data analysis was performed using the Nova software (NT-MDT).

Two types of purified SWCNTs were used in this study and were labelled as type A (HiPCo, Carbon Nanotechnology Inc.) and type B (P2-SWNT, Carbon Solutions). SWCNTs were sonicated in solvent (chloroform) for 10 min followed by spreading on a thin glass coverslip. The solvent was evaporated at room temperature. After all the solvent had evaporated, the coverslip with SWCNT was placed on the AFM stage which was integrated with the inverted microscope. An area with dispersed SWCNT was scanned using the confocal Raman mode. The laser spot was positioned at the area that produced a strong SWCNT signal to ensure that some of the SWCNTs were illuminated within the laser spot. The illuminated area of the sample was then scanned by the gold-coated AFM tip in contact mode. Whenever the tip entered the laser spot, an apparent increase in fluorescent background was noticed. In cases where the tip was TERS active, the area where SWCNT was present showed an enhanced Raman signal of the SWCNT. This is generally used as the 'hot spot' for scanning. Figure 1 shows an example of a hot spot and the corresponding AFM image which were obtained simultaneously. The bright area in the Raman map coincides with the presence of SWCNTs shown in the AFM image. The tip was fixed at the 'hot spot' while TERS maps were obtained by moving the sample (maximum range is  $\sim 100 \mu\text{m} \times 100 \mu\text{m}$ ).

### 3. Results and discussion

To demonstrate the TERS effect, an image of dispersed SWCNT (pure type A SWCNT) was first scanned with, then

without a tip. A chemical image of the SWCNT has been generated from the data by plotting the G band intensity at  $1596 \text{ cm}^{-1}$  across the scanned area. The background is subtracted from the intensity image to remove the unwanted shift in baseline during measurements. The scan without the tip (tip retracted) shows a relatively broad feature with blurred edges (figure 2(B)). The G band signal has  $\sim 40$  counts under the defined measurement conditions. The image from the scan with tip in contact reveals sharper outlines of the SWCNT. An intensity profile across dispersed SWCNTs shows that the spatial resolution achieved was  $\sim 14$  nm. This was higher than previously reported [6] using a similar system apparently because of the smaller step size used in this experiment and was similar to the spatial resolution reported by others using different instruments [14–16]. The 4 nm spatial resolution reported by Yano *et al* [9] was achieved by measuring peak shift rather than Raman intensity and the high spatial resolution observed resulted from the mechanical effect on the sample under localized contact pressure. The enhanced spatial resolution compared to the far-field confocal measurement demonstrated in figure 2 is the result of the localized enhancement of Raman intensity at the apex of the tip. Note that the G band intensity from the image with the tip approaching is  $\sim 120$  counts which is  $\sim 3\times$  the signal compared to the measurements without the tip. On some occasions ( $\sim 10\%$  of the tips), when a relatively high power laser was used ( $\sim 1$  mW) a very strong enhancement of Raman signal ( $\sim 70\times$ , comparing the G band intensity between the tip approaching and retracting) from the tip can be observed. However, the signal decays rapidly when such strong enhancement occurs and eventually the entire enhancement is lost. The power of the laser at the tip is important for experiments with longer acquisition time. The tip property was found to be changing continuously with higher laser intensities. The instability of the tip with high laser power is thought to be caused by heating of the tip [17] which could induce physical instability of the gold coating. Under such conditions, the gold coating may form shapes that can produce high TERS signals for a short period of time. When the gold-coated tip is exposed in high laser intensity for a longer period of time (several

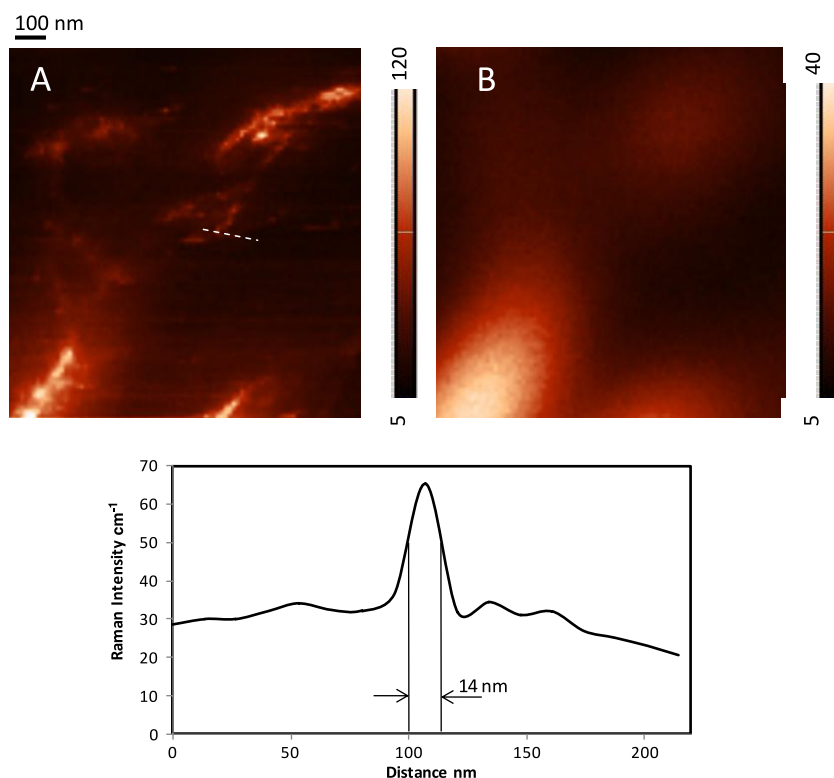


**Figure 2.** TERS image of dispersed SWCNTs, type A. The images are generated based on the intensity of the SWCNT G band at  $1596\text{ cm}^{-1}$ . Image (A) shows the result when the tip is approaching. Image (B) shows the result when tip is retracted. The plot has shown the Raman intensity profile along the dotted line marked on (A).

minutes), the Si peak intensity from the AFM tip increases, suggesting the gold is eventually evaporated resulting in a loss in TERS signal. Although the enhancement was very strong for those tips, it was not considered to be suitable for the scanning TERS experiment as a stable enhancement for a long exposure time under the laser light illumination is required. When weaker enhancement was observed, the enhanced signal was found to be more stable and the tip remained active for a few days as was the case with the results shown in figure 2. When the enhancement is eventually lost due to wear or contamination of the tip (since the scan is operated in contact mode) the tip can be recoated by gold sputtering and the enhancement effect may be re-established. However, our experience has shown that the recoated tip often gives a lower enhancement level compared to newly coated tips, possibly due to the increased thickness of gold causing an increase in diameter of the recoated tip apex. Nevertheless, a strong enhancement is not a requirement for studying SWCNTs. In our setup, the maximum laser power that could be used before the tip became unstable was  $\sim 0.05\text{ mW}$ . To prolong the life of an active tip,  $0.01\text{ mW}$  laser power was used and the result obtained has shown that this level of laser power is sufficient for mapping SWCNTs. In fact, the image shown in figure 2(A) contains both far-field as well as TERS signals. Apparently, a clear TERS image of SWCNTs can be produced with the current level of enhancement. From the Raman spectrum of the pure type A nanotube shown in figure 3(A), several bands in the RBM region can be noticed suggesting that this SWCNT

type, despite being purified, contains nanotubes of different diameters. Another scanning TERS map (see figures 3(B)–(D)) of the pure type A SWCNT on a glass cover slip with smaller step size has revealed a heterogeneous distribution of nanotubes of different diameters, which was generated using the bands at  $287$  and  $264\text{ cm}^{-1}$ . This demonstrates that scanning TERS is suitable to detect different SWCNTs with various diameters within a bundle.

After establishing a TERS image with the set up described, scanning TERS was applied to analyse SWCNTs that were intentionally contaminated with a different SWCNT (type B). The spectrum of type B SWCNT is overlapped with the spectrum of type A in figure 3(A). The shape of the G bands indicates that type A is a semiconducting SWCNT, while type B is a metallic SWCNT [18]. The other main spectral differences between the two SWCNTs are found at the RBM in the lower wavenumber regions due to the large difference in diameters between the two SWCNTs [12, 19, 20]. The diameter distribution of the type B SWCNT appears to be less diverse and the RBM has a wavenumber significantly lower than type A. These differences in spectral features allow images corresponding to the distribution of the contaminated SWCNT to be generated. Figure 4 shows the result of the measurement of the ‘contaminated’ SWCNT bundles. The AFM topography image shows the outline of the SWCNT (figure 4(A)). However, it contains no chemical information that may be used to distinguish the two different SWCNTs. The TERS image based on the G band ( $1596\text{ cm}^{-1}$ ) clearly

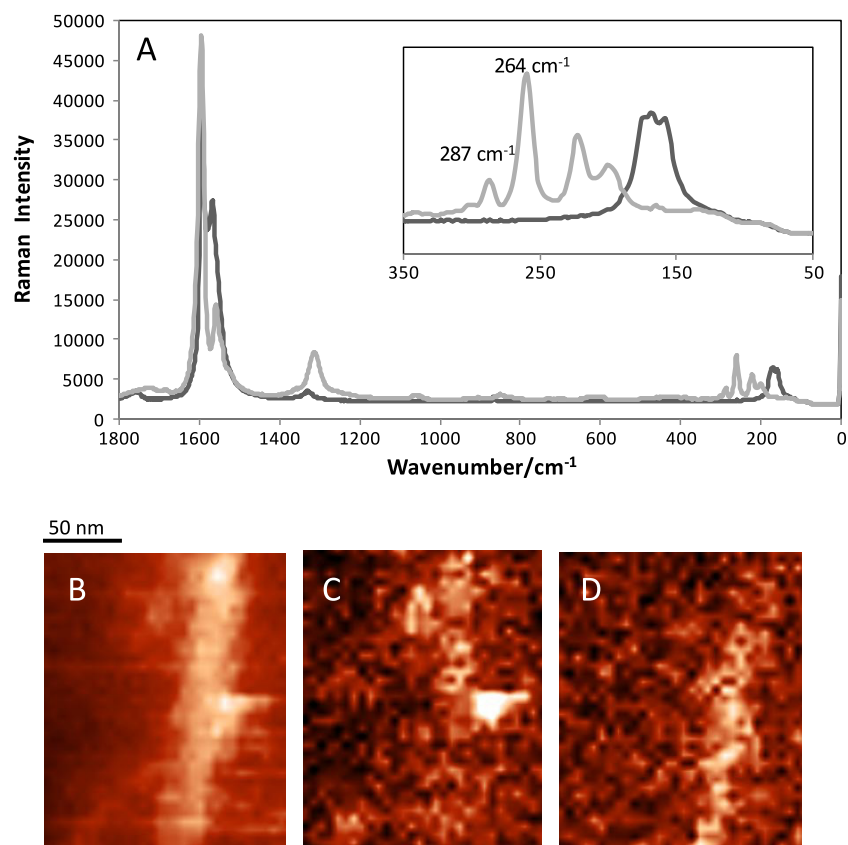


**Figure 3.** (A) Raman spectra of type A (grey line) and type B (dark grey line) SWCNTs measured using a confocal Raman microscope. The inset shows the expanded spectral region for the RBM vibrations of the two SWCNTs. (B), (C) and (D) are the scanning TERS images of the dispersed pure type A SWCNT generated by plotting the intensity of the G band ( $1595\text{ cm}^{-1}$ ), the band from RBM at  $287\text{ cm}^{-1}$  and  $264\text{ cm}^{-1}$  across the measured area, respectively.

outlines all the SWCNTs as shown in figure 4(B). The presence of SWCNT was detected and the location coincided well with the topography image. The tip used to obtain these images was a recoated tip and the level of enhancement is smaller than with a newly coated tip, as demonstrated in figure 2(A). The TERS image generated by the Raman band due to the RBM vibration at  $\sim 173\text{ cm}^{-1}$ , which is specific to the contaminant SWCNT (type B), reveals the location of this type of SWCNT (figure 4(C)). Note that despite type A containing SWCNTs of several diameters, in all the TERS maps of pure type A sample no SWCNT was found with a Raman spectral band at  $\sim 173\text{ cm}^{-1}$ . From these images, one can deduce that the type B SWCNT mostly appeared at the peripheral area around the main bundle. The result demonstrates that chemically specific Raman spectra can help to identify different SWCNTs in the mixture with spatial resolution similar to an AFM measurement. Note that due to the weaker enhancement level compared to the measurement shown in figure 2, the far-field Raman signal appears to be stronger, especially in the area where the SWCNT bundle is thickest. However, the more dispersed SWCNT at the peripheral area of the bundle seems to be less affected by the far-field signal. A high TERS signal can be produced from a small bundle while the far-field signal from the same bundle is very small. On the other hand, a similar level of TERS signal would be expected from a much larger

bundle due to the small enhancement zone for TERS while the far-field signal is stronger for the larger bundle.

It is interesting to note that a few of the 'SWCNTs' that were detected in the TERS images did not appear on the AFM topography image (indicated by the white arrows in figures 4(B) and (C)). One of the possible reasons for this is the temporary sticking of small SWCNTs on the hot spot. This is characterized by the appearance of the enhanced signal in a straight horizontal line. Another possible reason is that the feature was too thin to be detected with the slow AFM scan. Under normal operation, the AFM system can detect thin samples such as single layer graphene. However, when the topographic image was recorded during TERS measurement, the peak to peak noise level was increased due to the slow scanning speed. Raman spectra extracted from the region indicated by the arrow in figure 4(B) show an enhanced signal with a strong D band. When the D band at  $1320\text{ cm}^{-1}$  was used to generate the TERS image, the line indicated by the white arrow in figure 4(B) is more clearly seen in the image in figure 4(D). The higher intensity of the D band can be an indication of the presence of amorphous carbon [18, 21]. The result suggests that the imaged area was contaminated with amorphous carbon, which may also explain the lack of SWCNT-like topographic features in that area.

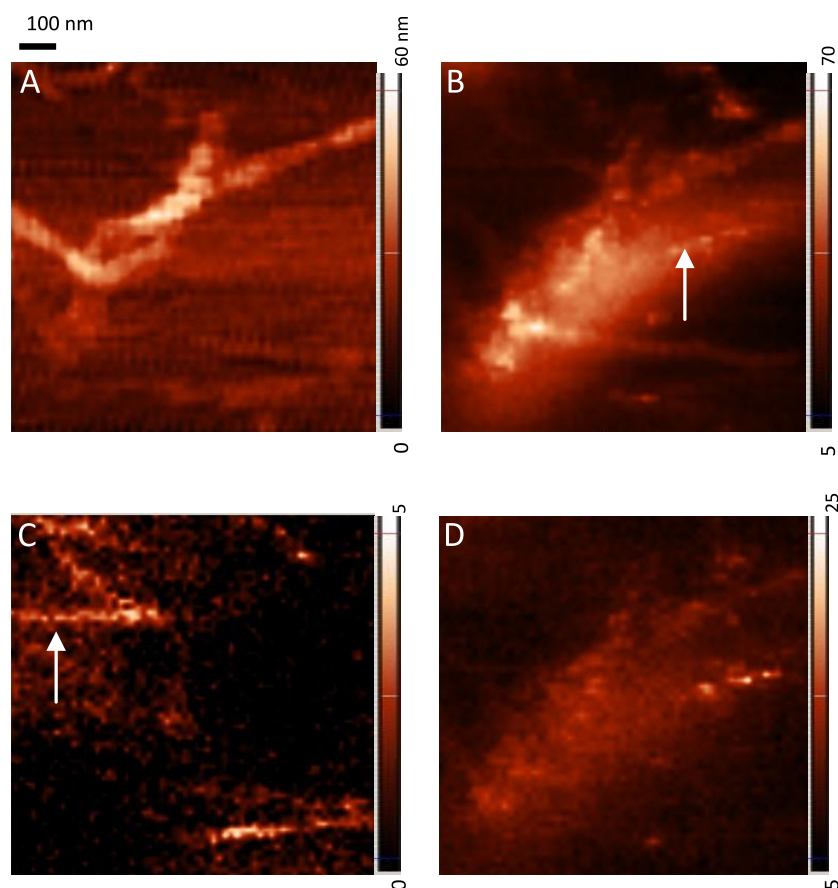


**Figure 4.** Images measured simultaneously with the gold-coated tip approaching sample. (A) An AFM topographic image of the measured area of the dispersed SWCNT mixture. (B) TERS image of the SWCNT based on the G band at  $1596\text{ cm}^{-1}$ . (C) TERS image of the SWCNT based on the radial breathing mode specific to the contaminant SWCNT at  $\sim 173\text{ cm}^{-1}$  (type B). (D) TERS image of the SWCNT based on the D band at  $\sim 1320\text{ cm}^{-1}$  highlighting an area of amorphous carbon.

#### 4. Conclusions

In conclusion, it has been shown that TERS is a very useful tool for chemical analysis of nanometre scale materials with a demonstrated spatial resolution of 14 nm. Relatively small enhancement ( $\sim$ three times) is shown to be adequate, even beneficial, for the imaging of SWCNTs. Tip stability was found to decrease dramatically when a higher power laser was used. We have demonstrated the application of scanning TERS to detect and locate SWCNTs of the same type but different diameters (a single batch) and the contaminant SWCNT near a bundle of different types of SWCNTs. Nanosize amorphous carbon contaminant can also be detected using this method. Differentiation of carbon nanotubes with different diameters in a prepared mixture was possible for the first time due to the chemical specificity of Raman scattering and high spatial resolution obtained using a gold-coated AFM tip.

#### Acknowledgments

SGK acknowledges the research funding from the European Research Council under the European Community's Seventh Framework Programme (FP7/2007-2013)/ERC advanced grant agreement no. [227950] and we thank NT-MDT.

#### References

- [1] Jeanmaire D L and Van Duyne R P 1977 Surface Raman spectroelectrochemistry. 1. Heterocyclic, aromatic, and aliphatic-amines adsorbed on anodized silver electrode *J. Electroanal. Chem.* **84** 1–20
- [2] Stockle R M, Suh Y D, Deckert V and Zenobi R 2000 Nanoscale chemical analysis by tip-enhanced Raman spectroscopy *Chem. Phys. Lett.* **318** 131–6
- [3] Yeo B S, Schmid T, Zhang W H and Zenobi R 2007 Towards rapid nanoscale chemical analysis using tip-enhanced Raman spectroscopy with Ag-coated dielectric tips *Anal. Bioanal. Chem.* **387** 2655–62
- [4] Hartschuh A, Qian H, Georgi C, Bohmler M and Novotny L 2009 Tip-enhanced near-field optical microscopy of carbon nanotubes *Anal. Bioanal. Chem.* **394** 1787–95
- [5] Roy D, Wang J and Welland M E 2006 Nanoscale imaging of carbon nanotubes using tip enhanced Raman spectroscopy in reflection mode *Faraday Discuss.* **132** 215–25
- [6] Kharintsev S S, Hoffmann G G, Dorozhkin P S, de With G and Loos J 2007 Atomic force and shear force based tip-enhanced Raman spectroscopy and imaging *Nanotechnology* **18** 315502
- [7] Zhang W H, Cui X D, Yeo B S, Schmid T, Hafner C and Zenobi R 2007 Nanoscale roughness on metal surfaces can increase tip-enhanced Raman scattering by an order of magnitude *Nano Lett.* **7** 1401–5

- [8] Pettinger B, Domke K F, Zhang D, Picardi G and Schuster R 2009 Tip-enhanced Raman scattering: influence of the tip-surface geometry on optical resonance and enhancement *Surf. Sci.* **603** 1335–41
- [9] Yano T, Verma P, Saito Y, Ichimura T and Kawata S 2009 Pressure-assisted tip-enhanced Raman imaging at a resolution of a few nanometres *Nat. Photon.* **3** 473–7
- [10] Shelimov K B, Esenaliev R O, Rinzler A G, Huffman C B and Smalley R E 1998 Purification of single-wall carbon nanotubes by ultrasonically assisted filtration *Chem. Phys. Lett.* **282** 429–34
- [11] Medjo R E, Sendja B T, Mane J M and Ateba P O 2009 A study of carbon nanotube contamination by XANES spectroscopy *Phys. Scr.* **80** 6
- [12] Jorio A, Saito R, Hafner J H, Lieber C M, Hunter M, McClure T, Dresselhaus G and Dresselhaus M S 2001 Structural (n, m) determination of isolated single-wall carbon nanotubes by resonant Raman scattering *Phys. Rev. Lett.* **86** 1118–21
- [13] Anderson N, Hartschuh A and Novotny L 2007 Chirality changes in carbon nanotubes studied with near-field Raman spectroscopy *Nano Lett.* **7** 577–82
- [14] Steidtner J and Pettinger B 2008 Tip-enhanced Raman spectroscopy and microscopy on single dye molecules with 15 nm resolution *Phys. Rev. Lett.* **100** 4
- [15] Cancado L G, Hartschuh A and Novotny L 2009 Tip-enhanced Raman spectroscopy of carbon nanotubes *J. Raman Spectrosc.* **40** 1420–6
- [16] Anderson N, Hartschuh A, Cronin S and Novotny L 2005 Nanoscale vibrational analysis of single-walled carbon nanotubes *J. Am. Chem. Soc.* **127** 2533–7
- [17] Zhang W H, Schmid T, Yeo B S and Zenobi R 2008 Near-field heating, annealing, and signal loss in tip-enhanced Raman spectroscopy *J. Phys. Chem. C* **112** 2104–8
- [18] Jorio A, Pimenta M A, Souza A G, Saito R, Dresselhaus G and Dresselhaus M S 2003 Characterizing carbon nanotube samples with resonance Raman scattering *New J. Phys.* **5** 17
- [19] Dresselhaus M S, Dresselhaus G, Saito R and Jorio A 2005 Raman spectroscopy of carbon nanotubes *Phys. Rep.* **409** 47–99
- [20] Yano T, Verma P, Kawata S and Inouye Y 2006 Diameter-selective near-field Raman analysis and imaging of isolated carbon nanotube bundles *Appl. Phys. Lett.* **88** 093125
- [21] Hayazawa N, Yano T, Watanabe H, Inouye Y and Kawata S 2003 Detection of an individual single-wall carbon nanotube by tip-enhanced near-field Raman spectroscopy *Chem. Phys. Lett.* **376** 174–80